PRAMANA
— journal of
physics

Vol. 74, No. 6
June 2010
pp. 1017–1027

Electronic properties and Compton profiles of silver iodide

ALPA DASHORA[1], AMBICA MARWAL[2], K R SONI[2] and B L AHUJA[1,*]
[1]Department of Physics, University College of Science, M.L. Sukhadia University, Udaipur 313 001, India
[2]Department of Physics, Malaviya National Institute of Technology, Jaipur 302 017, India
[*]Corresponding author. E-mail: blahuja@yahoo.com

MS received 24 December 2009; revised 13 February 2010; accepted 19 February 2010

Abstract. We have carried out an extensive study of electronic properties of silver iodide in β- and γ-phases. The theoretical Compton profiles, energy bands, density of states and anisotropies in momentum densities are computed using density functional theories. We have also employed full-potential linearized augmented plane-wave method to derive the energy bands and the density of states. To compare our theoretical data, isotropic Compton profile measurement on γ-AgI using ^{137}Cs Compton spectrometer at an intermediate resolution of 0.38 a.u. has been undertaken. The theoretical anisotropies are also interpreted on the basis of energy bands.

Keywords. X-ray scattering; band structure calculations; density functional theory; semiconductors.

PACS Nos 13.60.Fz; 71.15.Ap; 72.80.Ey; 78.70.Ck

1. Introduction

The physical and chemical properties of silver iodide (AgI) have been studied due to its pronounced applications in solid-state batteries, photographic films, visible range detectors, liquid semiconductors, cloud condensation, etc. [1–10]. At the ambient temperature, this compound remains in γ-phase [11]. Both the β- and γ-AgI transform to body-centred-cubic (bcc) α-AgI at 420 K [12]. The α-AgI is stable above this temperature and remains in the superionic phase [13], because the Ag ions can move through the bcc lattice of I ions.

Among earlier theoretical studies, Victora [14] has used the full-potential linear augmented Slater-type orbital (FP-LASTO) method within local density approximation (LDA) scheme to calculate the electronic structures of three polymorphs of AgI. The electronic structures of β- and γ-AgI have been presented by Vogel *et al* [15] by employing self-interaction correction (SIC) and self-interaction and relaxation correction (SIRC) to pseudopotentials together with Gaussian-orbital basis

sets. Laref *et al* [16] have used empirical tight binding (TB) method and calculated the electronic properties of γ-AgI. Okoye [17] has investigated the pressure dependence of band gaps for some silver halides. Recently, Ono *et al* [18] have studied the electronic structure and diffusion paths of Ag ions in rock salt (RS) structured AgI using full-potential linear muffin-tin orbital (FP-LMTO) method within the generalized gradient approximation (GGA) scheme. In addition, some experimental studies to probe different properties of AgI have also been reported by different workers [19–23].

It is well established that the Compton profile $J(p_z)$ is a spectrum of inelastically scattered photons by the target's electrons. It can be used to probe the electronic structure of a variety of materials [24]. The theoretical $J(p_z)$ is defined as the one-dimensional projection of electron momentum density $\rho(p_z)$, along the scattering vector (z-axis) direction. In Compton experiments, one measures the double differential cross-section that is related to $J(p_z)$ as follows [24]:

$$\frac{\mathrm{d}^2\sigma}{\mathrm{d}\Omega\,\mathrm{d}\omega} \propto J(p_z) = \iint \rho(\vec{p})\mathrm{d}p_x\,\mathrm{d}p_y. \tag{1}$$

To shed more light on the electronic structure of AgI, in this paper we report the energy bands and the corresponding density of states (DOS) using the linear combination of atomic orbitals (LCAO) and the full-potential linearized augmented plane-wave (FP-LAPW) method. We have also computed, for the first time, the Compton line shapes using density functional theory (DFT) within the LDA and GGA, and also hybridization of Hartree–Fock (HF) and DFT (so-called B3LYP) schemes using LCAO method. To compare the data on momentum densities, we have also measured the isotropic Compton profile of γ-AgI using ^{137}Cs isotope.

2. Methods

2.1 *Experiment*

The isotropic experimental Compton profile of γ-AgI was carried out using a high energy (662 keV) ^{137}Cs Compton spectrometer [25] at an intermediate momentum resolution of 0.38 a.u. (Gaussian full-width at half-maximum), which is better than that of the conventional ^{241}Am spectrometer. The energy spectra of the scattered γ-rays at an angle of $160\pm0.6^\circ$ were measured by a high-purity Ge detector (Canberra, GL0210P) and associated electronics. Due to the non-availability of large size (12 mm diameter and 2 mm thickness) single crystal, we have only measured the isotropic Compton profile. The polycrystalline sample of AgI (12 mm diameter and 2.2 mm thickness) was exposed for 218 h to obtain sufficient statistics in the Compton data. The raw line shape data were accumulated by a 4 K channel analyser (Canberra, Accuspec B) with a channel width of about 61 eV. To derive the true Compton profile, the energy distribution of inelastically scattered spectra were corrected for background, instrumental resolution (limited to stripping off the low energy tail), detector efficiency, Compton cross-section, multiple scattering, etc. [24]. To measure the background experimentally, the experiment is performed without sample and the measured background data are then subtracted from the

selected range of the sample data, channel by channel, after scaling it to the actual measuring time of the sample data. In the present study, the ratio of multiple to single scattering events (in the momentum range −10 to +10 a.u.) was found to be 10.6%. It is worthwhile to mention that we have incorporated the multiple scattering correction upto triple scattering. The contribution from the higher-order scattering is expected within the statistical errors of the experiment. Further, as suggested by our group [26], we have also corrected the experimental profile for the bremsstrahlung (BS) background due to photo and Compton recoiled electrons liberated in the sample. Finally, the profile was transformed from energy to momentum scale and normalized to the free atom Compton profile (range 0 to 5 a.u.) area of 35.6 electrons [27].

2.2 *Theory*

2.2.1 *LCAO method*

In the present paper, we have employed the CRYSTAL03 package [28] for the computation of Compton profiles, energy bands and DOS of β- and γ-AgI. The code is based on LCAO method and uses basis sets of Slater-type orbitals (STOs), which are approximated by orbitals of Gaussian-type.

The electron density $\rho(\vec{r})$ of an N-electron system described by this type of wave function is given from the optimum one-electron crystalline orbital ϕ_j^k by

$$\rho(\vec{r}) = \int_{\mathrm{BZ}} \mathrm{d}\vec{k} \sum_j |\phi_j^k| \theta(\varepsilon_{\mathrm{F}} - \varepsilon_j(\vec{k})), \tag{2}$$

where $\varepsilon_j(\vec{k})$ is the k-dependent eigenvalue of the jth crystalline orbital, θ is the heaviside step function, ε_{F} is the Fermi energy and $\vec{k}$ is the generating vector of the irreducible representation of the group of crystal translations.

Various approximations, namely, DFT (with LDA and GGA) and B3LYP as incorporated in this single package differ in the form of monoelectronic Hamiltonian operator $\hat{h}$. In the Kohn–Sham (KS) formulation of DFT, the exchange-correlation potential operator is defined in terms of exchange-correlation energy per particle in uniform interacting electron gas of density ρ. The Hamiltonian operator in this case becomes

$$\hat{h}_{\mathrm{KS}} = \hat{T} + \hat{V} + \hat{J}[\rho(\vec{r})] + \hat{v}_{\mathrm{XC}}(\vec{r}), \tag{3}$$

where $\hat{T}$, $\hat{V}$, $\hat{J}$ and $\hat{v}_{\mathrm{XC}}$ are the kinetic, external potential, Coulomb and exchange operators, respectively.

The exchange-correlation potential operator, $\hat{v}_{\mathrm{XC}}(\vec{r})$ is the functional derivative of the exchange correlation density functional energy, E_{XC}, with respect to charge density at a point $\vec{r}$. Within LDA, E_{XC} is defined as

$$E_{\mathrm{XC}} = \int_{\text{unit cell}} \mathrm{d}r \varepsilon_{\mathrm{XC}}[\rho(\vec{r})]. \tag{4}$$

Table 1. Different exchange and correlation functionals used in the present LCAO calculations.

Theory	Exchange	Correlation
DFT-LDA	Dirac–Slater [28]	Perdew–Zunger [29]
DFT-GGA	Becke [30]	Perdew–Wang [31,32]
B3LYP	Becke [30]	Lee–Yang–Parr [33]

In GGA,

$$E_{\mathrm{XC}} = \int f(\rho(\vec{r}), |\Delta\rho(\vec{r})|)\mathrm{d}r, \tag{5}$$

in which $f(\rho(\vec{r}), |\Delta\rho(\vec{r})|)$ is a suitably chosen function of its two variables. A summary of various exchange and correlation functionals [28–33] used in the present calculations is listed in table 1.

In the present calculations, all-electron basis sets of Gaussian-type orbitals (GTOs) for Ag and I have been taken from ref. [34]. These basis sets were optimized using BILLY software. For a faster convergence of self-consistent-field (SCF) cycles, the BROYDEN scheme [35] was applied for all the calculations. The integration in the reciprocal space has been carried out on a grid of 216 $\vec{k}$ points for β-AgI and γ-AgI in the irreducible BZ. The lattice parameters for β-AgI were taken to be $a = 4.599$ and $c = 7.524$ Å, while in the case of γ-AgI, a was 6.499 Å [23]. In order to make a direct comparison of our experiment with the theoretical momentum densities, the computed valence Compton profiles have been added to free atom core contribution [27].

2.2.2 *FP-LAPW method*

The FP-LAPW (+ local orbitals) method within the DFT scheme [36] has been used for the computation of electronic structures of β- and γ-AgI. In the LAPW method, the space is divided into non-overlapping muffin-tin (MT) spheres centred at the atomic sites and an interstitial region. In the interstitial region, the basis set is described by plane waves. In the MT spheres, it is treated by radial solutions of the one-particle Schrödinger equation at fixed energies and their energy derivatives time spherical harmonics. In this method, the band structure calculations are expected to be accurate because no shape approximation is made for the charge density or potential. In the present work, the latest non-empirical DFT-GGA methodology of Wu and Cohen [37] has been used for the first time. The convergence criterion for total energy was set to 0.1 mRy with cut-off charge density $G_{\max} = 12$. Density plane wave cut-off $R_{\mathrm{MT}}K_{\max}$ was kept equal to 7, which controls the convergence of the basis set. The radial basis functions of each LAPW were calculated up to $l_{\max} = 10$. In the present calculations, 114 and 73 $\vec{k}$ points were taken for β- and γ-AgI, respectively in the irreducible wedge of BZ. For both phases of AgI, the MT sphere radii used were 2.5 a.u. for Ag and I.

3. Results and discussion

3.1 *Energy bands and DOS*

In figures 1–4, we have presented the dispersion of the calculated energy bands (E–k relations) along some high symmetry directions in the BZ and also the total and partial DOS of γ- and β-AgI using the LCAO (GGA) and FP-LAPW methodologies. A solid horizontal line in the energy band diagram shows the position of Fermi energy (E_F). Due to similar topological nature of energy bands within LDA and B3LYP schemes of the LCAO method, only E–k relations corresponding to GGA calculations are shown here. Except some fine structures and band gaps, the overall shape of our energy bands is in agreement with the earlier reported data [14–16].

From figures 1–4, it is observed that the energy bands of AgI can be divided into three main groups. The lowest bands in the valence region originate primarily due to the 5s states of I. In both the phases, within FP-LAPW approximation, these bands lie at around −12 to −13 eV. The valence band maximum (VBM) is formed due to hybridization of 4d states of Ag and 5p states of I leading to degenerate states. This degeneracy leads to very strong p–d hybridization in wave functions and a considerable complexity in the VB structure as revealed in figures 1–4. Here we can see that the spatial extent of the Ag d levels is large, and their energies are close to those of the p levels of I. The p and d levels therefore hybridize and alter the chemical behaviour of this compound significantly. The conduction band minimum

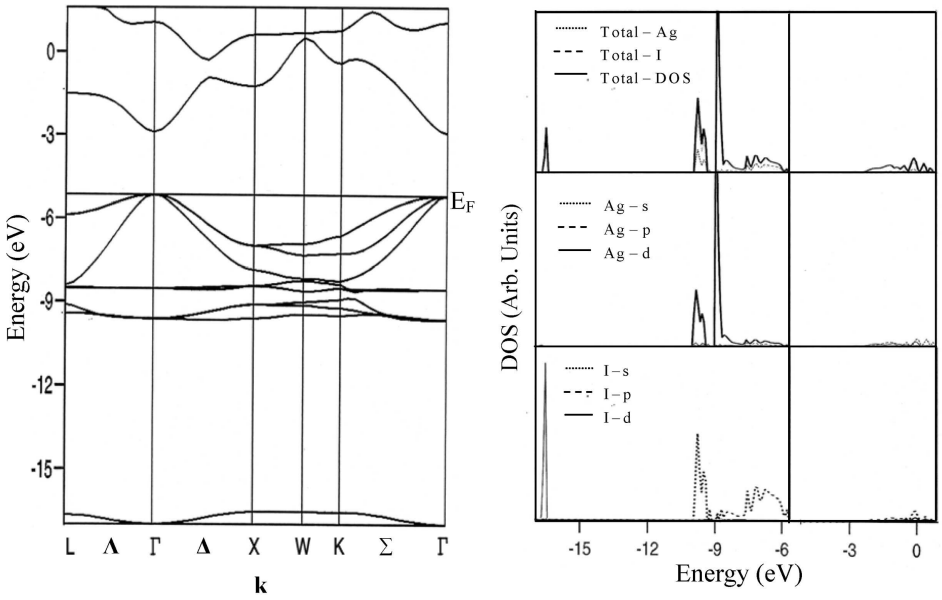

Figure 1. Band structure (E–k relation) and density of states of γ-AgI along high symmetry directions of the first Brillouin zone within DFT-GGA scheme of LCAO method. The positions of the L, Γ, X, W and K vertices correspond to (0, 0, 1/2), (0, 0, 0), (0, 1/2, 1/2), (1/4, 1/2, 1/4) and (3/8, 3/8, 3/4), respectively.

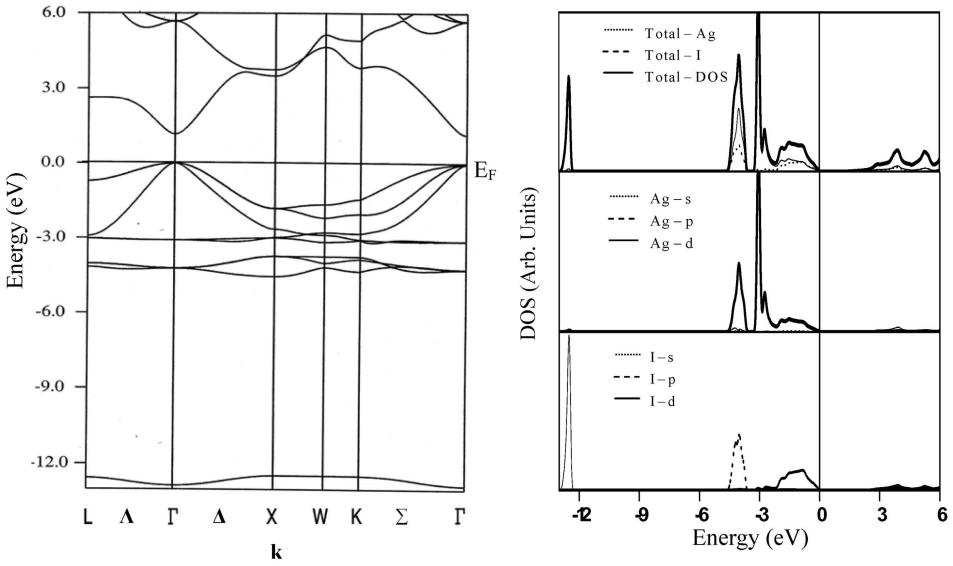

Figure 2. Same as figure 1 except the technique, which is FP-LAPW (GGA). In the Wien2k package, E_F is taken as the zero reference level.

(CBM) seems to originate from the s states of Ag with a small contribution from p and d orbitals of I. The band gap depends weakly on I in AgI, because the VBM is an Ag p-like state and the CBM is Ag s-like. Since β-AgI has four atoms per unit cell, the number of bands observed with this structure is double (figures 3 and 4) that of γ-AgI (figures 1 and 2). The results show that AgI is a direct band gap semiconductor (at Γ point).

The difference between the band structure calculations on rock-salt (RS) structured semiconductors (AgCl and AgBr) and AgI is that the former are indirect gap semiconductors with the VBM at the L point and the CBM at the Γ point [20] of the BZ, whereas β- and γ-AgI are direct band gap semiconductors. The reason for the difference between AgCl and AgBr and their tetrahedral counterpart AgI is the inversion symmetry of the RS lattice. The numerical values of energy band gap at Γ point of the present calculations and the available data are quoted in table 2. Our DFT-LDA and GGA theories give band gaps smaller than the experimental values reported in [21,22] for β- and γ-AgI, respectively, whereas our B3LYP scheme is in good agreement with these values. Other theoretical calculations performed by Victora [14] and Vogel *et al* [15] underestimate the experimental values and are comparable to our FP-LAPW calculations.

3.2 *Compton profiles*

The anisotropies in the momentum densities computed from the directional Compton profiles within the framework of DFT (with LDA and GGA) and B3LYP schemes are plotted in figures 5a and b for γ- and β-AgI, respectively. These figures

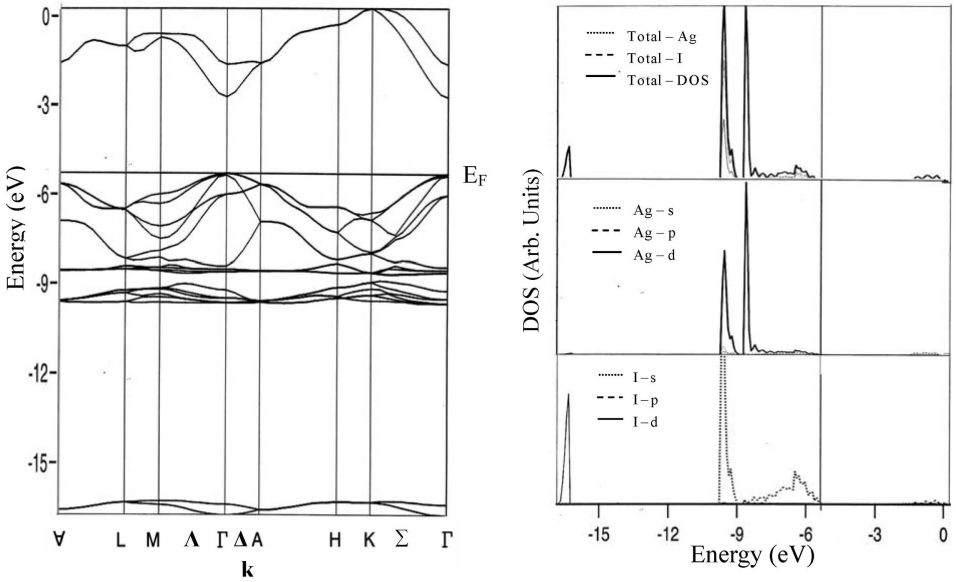

Figure 3. *E–k* relations and density of states of β-AgI using LCAO-DFT-GGA. The positions of the A, L, M, Γ, H and K vertices are (0, 0, 1/2), (1/2, 0, 1/2), (1/2, 0, 0), (0, 0, 0), (1/3, 1/3, 1/2) and (1/3, 1/3, 0), respectively.

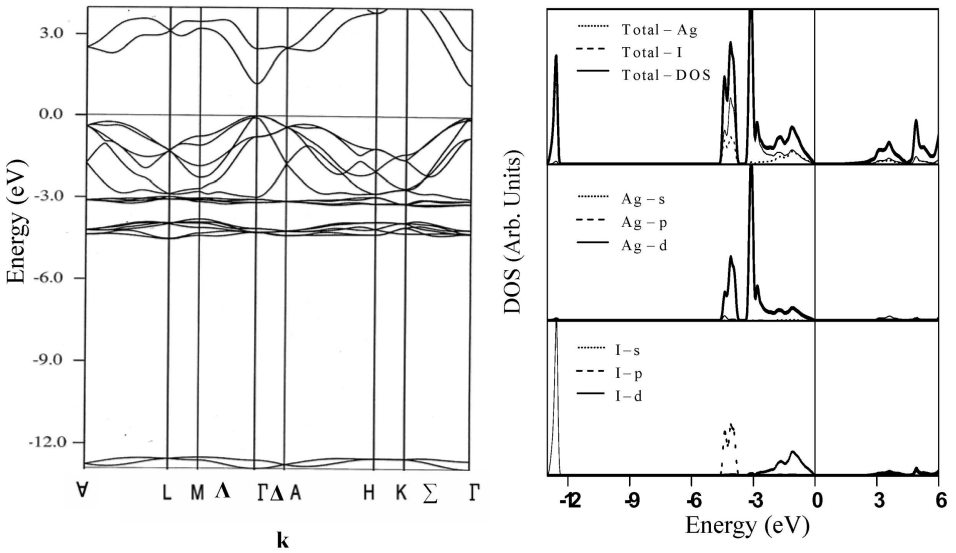

Figure 4. Same as figure 3 except the technique, which is FP-LAPW (GGA).

show that the general trend of oscillations in the unconvoluted theoretical Compton profile anisotropies for γ- and β-AgI differs at various values of p_z. The anisotropies in the momentum densities can be explained on the basis of one-electron energies

Table 2. Band gaps (ΔE_g) of β- and γ-AgI in electron volts.

		ΔE_g	
Method		β-AgI	γ-AgI
(i) *Present work*			
(a) LCAO	DFT-LDA	1.72	1.91
	DFT-GGA	1.82	2.26
	B3LYP	2.91	3.69
(b) FP-LAPW		1.20	1.17
(ii) *Available data*	FP-LASTO	1.5 [14]	1.4 [14]
	PP	0.8 [15]	0.8 [15]
	SIRC (PP)	1.5 [15]	1.4 [15]
	Expt.	3.0 [22]	2.82 [21,14]

SIRC: Self-interaction and relaxation correction.
FP-LASTO: Full-potential linear augmented Slater-type orbital.

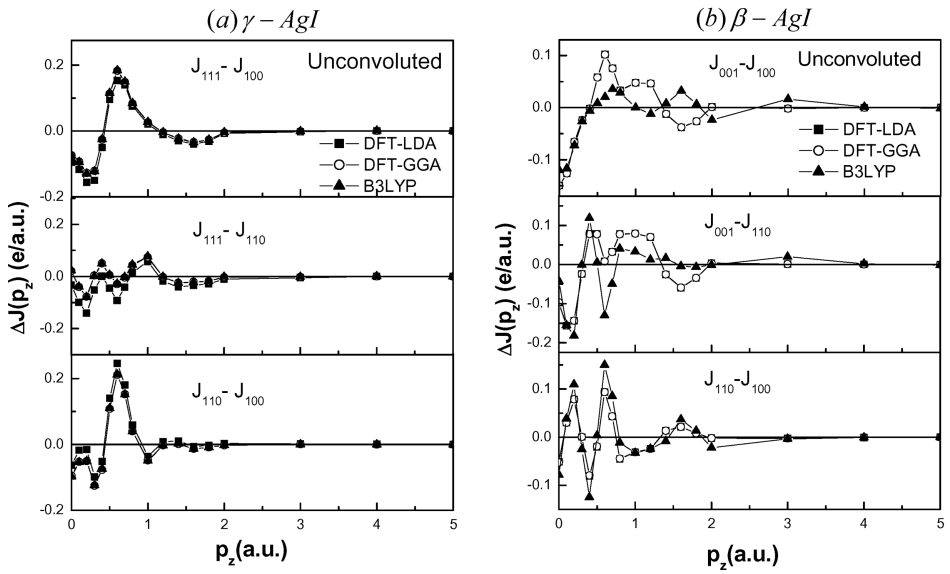

Figure 5. Anisotropies in the unconvoluted and convoluted theoretical directional Compton profiles of (**a**) γ- and (**b**) β-phases of AgI computed using various schemes of CRYSTAL03 code. Solid lines are drawn to guide the eyes.

(energy bands). For example, in γ-AgI the energy bands (as shown in figure 1) contribute to fine structures in the momentum densities (figure 5a). There are degenerate states at the Γ point of the branch Γ-X, which leads to more momentum density at Γ point. Due to the non-existence of bands near E_F at the X point of the Γ-X branch, there is a deficit of momentum densities at Γ-X distance (0.51 a.u.)

Table 3. Experimental isotropic Compton profile of γ-AgI along with the spherically averaged theoretical Compton profiles calculated by various schemes of CRYSTAL03 code. The experimental error at few points is also shown. The theoretical profiles are unconvoluted.

p_z (a.u.)	LDA	GGA	B3LYP	Expt.
0	17.133	17.250	17.098	16.149±0.034
0.1	17.056	17.172	17.021	16.058
0.2	16.816	16.931	16.785	15.838
0.3	16.387	16.502	16.363	15.505
0.4	15.837	15.948	15.819	15.099
0.5	14.922	15.025	14.909	14.618
0.6	14.072	14.169	14.068	14.044
0.7	13.133	13.225	13.141	13.417
0.8	12.265	12.349	12.279	12.779
1.0	10.986	11.048	10.998	11.552±0.027
1.2	10.031	10.077	10.038	10.401
1.4	9.181	9.219	9.186	9.482
1.6	8.386	8.279	8.392	8.663
1.8	7.679	7.592	7.684	7.761
2.0	7.012	6.934	7.017	7.122±0.019
3.0	4.454	4.418	4.456	4.457±0.018
4.0	3.170	3.161	3.171	3.121±0.009
5.0	2.492	2.490	2.492	2.506±0.008

leading to a positive oscillation in the anisotropies with respect to [1 0 0] direction, as can be seen in figure 5a.

In table 3, we have given the isotropic experimental Compton profiles along with the unconvoluted theoretical profiles (spherically averaged) computed within the framework of DFT (LDA and GGA) and B3LYP techniques using LCAO method for γ-AgI. Before making a comparison with the experimental data, all the theoretical profiles were convoluted with the experimental resolution function of 0.38 a.u. The difference between the convoluted isotropic theoretical profiles (for γ-AgI) and the experimental profile is presented in figure 6. A good agreement in high momentum side ($p_z \geq 3$ a.u.) is due to the dominating contribution of core electrons, which are normally unaffected on the formation of solids. In low-momentum region ($p_z < 3$ a.u.), there are significant differences between the convoluted theories and the experiment. Such differences were also seen in the case of other Ag halides [20]. These significant differences need to be understood. In the vicinity of Compton peak, the B3LYP technique gives a marginally better agreement with the experimental momentum densities.

4. Conclusions

The electronic properties, namely energy bands and DOS, are presented using the LCAO and FP-LAPW methods. The isotropic experimental Compton profiles of

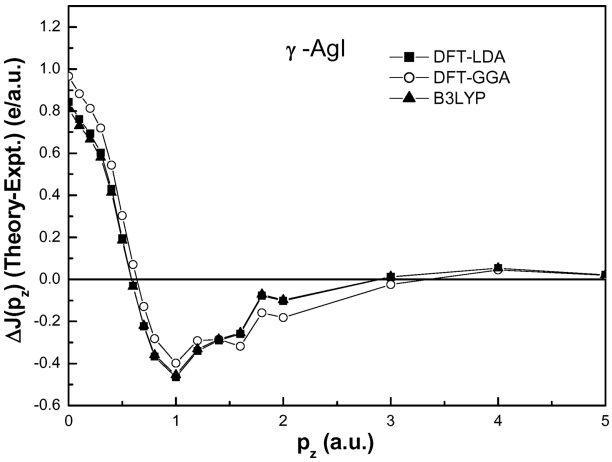

Figure 6. Difference between the isotropic experimental and the convoluted theoretical profiles using different LCAO schemes for γ-AgI. Statistical error is within the size of symbols used.

γ-AgI are compared with the LCAO calculations within the DFT schemes. It is seen that for γ-AgI, the B3LYP-based Compton line shape gives relatively a better agreement with the experimental electron momentum density, particularly in the low-momentum region. A disagreement in the vicinity of $p_z = 0$ may be due to the non-relativistic nature of the LCAO calculations. Except some fine structures, the computed energy bands of AgI within B3LYP approach are found to be in agreement with the experimental data. These calculations predict AgI to be a direct band gap semiconductor. To get more insight into the electronic structure of β- and γ-AgI, directional Compton profile measurements may be helpful.

Acknowledgements

The authors thank DST, New Delhi (India) and DRDO, New Delhi (India) for financial assistance. Prof. R Dovesi and Prof. P Blaha are thanked for providing the LCAO and FP-LAPW codes, respectively. We also acknowledge the help extended by Dr G Ahmed, Dr G Arora, Mr Vinit Sharma and Mr A Rathor during the experimental work.

References

[1] T H James (Ed.), *The theory of the photographic process* (Macmillan, New York, 1977)
[2] H Wiedersich and S Geller, *The chemistry of extended defects in non-metallic solids* (North-Holland, Amsterdam, 1970)
[3] W Van Gool (Ed.), *Fast ion transport in solids, solid state batteries and devices* (North-Holland, Amsterdam, 1973)

[4] G D Mahan (Ed.), *Superionic conductors: Chemistry, physics and applications* (Plenum, New York, 1976)
[5] J E Enderby and A C Barnes, *Rep. Prog. Phys.* **53**, 85 (1990)
[6] S Hull, *Rep. Prog. Phys.* **67**, 1233 (2004)
[7] X Guo, G Zheng and D Jin, *Atmos. Res.* **79**, 183 (2006)
[8] B L Davis and L H Adams, *Science* **146**, 519 (1964)
[9] S Hull, D A Keen and P Berastegui, *J. Phys.: Condens. Matter* **14**, R13579 (2002)
[10] M R Vukic, D S Veselinovic and V G Markovic, *J. Serb. Chem. Soc.* **72**, 857 (2007)
[11] J R G Patnaik and C S Sunandan, *J. Phys. Chem. Solids* **59**, 1059 (1998)
[12] J B Boyce and B A Huberman, *Phys. Rep.* **51**, 189 (1979)
[13] D A Keen, *J. Phys.: Condens. Matter* **14**, R819 (2002)
[14] R H Victora, *Phys. Rev.* **B56**, 4417 (1997)
[15] D Vogel, P Kruger and J Pollmann, *Phys. Rev.* **B58**, 3865 (1998)
[16] A Laref, W Sekkal, A Zaoui, M Certier and H Aourag, *J. Appl. Phys.* **86**, 4435 (1999)
[17] C M I Okoye, *Solid State Commun.* **129**, 69 (2004)
[18] S Ono, M Kobayashi, S Kashida and T Ohachi, *Solid State Ionics* **178**, 1023 (2007)
[19] A Goldmann, J Tejeda, N J Shevchik and M Cardona, *Phys. Rev.* **B10**, 4388 (1974)
[20] A Rathor, G Arora and B L Ahuja, *Phys. Status Solidi* **B245**, 1563 (2008)
[21] S Ves, D Glotzel, M Cardona and H Overhof, *Phys. Rev.* **B24**, 3073 (1981)
[22] W von der Osten, *Semiconductor physics of II–VI and I–VII compounds, semimagnetic semiconductors* edited by K H Hellwege and O Medelung (Landolt-Bornstein, New Series, Group III, Springer, Berlin, 1982) Vol. 17
[23] S Hull and D A Keen, *Phys. Rev.* **B59**, 750 (1999)
[24] M J Cooper, P E Mijnarends, N Shiotani, N Sakai and A Bansil, *X-ray Compton scattering* (Oxford Science Publications, New York, 2004) and references therein
[25] B L Ahuja, M Sharma and S Mathur, *Nucl. Instrum. Methods* **B244**, 419 (2006)
[26] S Mathur and B L Ahuja, *Phys. Lett.* **A335**, 245 (2004)
[27] F Biggs, L B Mandelsohn and J B Mann, *At. Data Nucl. Data Tables* **16**, 201 (1975)
[28] V R Saunders, R Dovesi, C Roetti, R Orlando, C M Zicovich-Wilson, N M Harrison, K Doll, B Civalleri, I J Bush, Ph D'Arco and M Llunell, *CRYSTAL2003 user's manual* (University of Torino, Torino, 2003)
[29] J P Perdew and A Zunger, *Phys. Rev.* **B23**, 5048 (1981)
[30] A D Becke, *Phys. Rev.* **A38**, 3098 (1988)
[31] J P Perdew and Y Wang, *Phys. Rev.* **B33**, 8800 (1986)
[32] J P Perdew and Y Wang, *Phys. Rev.* **B45**, 13244 (1992)
[33] C Lee, W Yang and R G Parr, *Phys. Rev.* **B37**, 785 (1988)
[34] http://www.tcm.phy.cam.ac.uk/∼mdt26/basis_sets
[35] D D Johnson, *Phys. Rev.* **B38**, 12807 (1988)
[36] P Blaha, K Schwarz, G Madsen, D Kvasnicka and J Luitz, *WIEN2k* (Vienna University of Technology, Vienna, Austria, 2001)
[37] Z Wu and R Cohen, *Phys. Rev.* **B73**, 235116 (2006)